Geochemistry Geophysics Geosystems G3
AN ELECTRONIC JOURNAL OF THE EARTH SCIENCES
Published by AGU and the Geochemical Society

Article
Volume 7, Number 11
22 November 2006
Q11019, doi:10.1029/2006GC001278
ISSN: 1525-2027

A GEOCLIM simulation of climatic and biogeochemical consequences of Pangea breakup

Y. Donnadieu
Laboratoire des Sciences du Climat et de l'Environnement, CNRS-CEA, CEA Saclay, Orme des Merisiers, Bat. 701, F-91191 Gif-sur-Yvette Cedex, France (yannick.donnadieu@cea.fr)

Department of Geophysical Sciences, University of Chicago, 5734 South Ellis Avenue, Chicago, Illinois 60637, USA

Y. Goddéris
LMTG, Observatoire Midi-Pyrénées CNRS, 14 Avenue Edouard Belin, F-31400 Toulouse, France

R. Pierrehumbert
Department of Geophysical Sciences, University of Chicago, 5734 South Ellis Avenue, Chicago, Illinois 60637, USA

G. Dromart
LST, Ecole Normale Supérieure, F-69364 Lyon Cedex 07, France

F. Fluteau
Institut de Physique du Globe de Paris, 4 Place Jussieu, Case 89, F-75252 Paris Cedex 05, France

R. Jacob
Mathematics and Computer Science Division, Argonne National Laboratory, 9700 South Cass Avenue, Argonne, Illinois 60439, USA

[1] Large fluctuations in continental configuration occur throughout the Mesozoic. While it has long been recognized that paleogeography may potentially influence atmospheric CO_2 via the continental silicate weathering feedback, no numerical simulations have been done, because of the lack of a spatially resolved climate-carbon model. GEOCLIM, a coupled numerical model of the climate and global biogeochemical cycles, is used to investigate the consequences of the Pangea breakup. The climate module of the GEOCLIM model is the FOAM atmospheric general circulation model, allowing the calculation of the consumption of atmospheric CO_2 through continental silicate weathering with a spatial resolution of 7.5°long × 4.5°lat. Seven time slices have been simulated. We show that the breakup of the Pangea supercontinent triggers an increase in continental runoff, resulting in enhanced atmospheric CO_2 consumption through silicate weathering. As a result, atmospheric CO_2 falls from values above 3000 ppmv during the Triassic down to rather low levels during the Cretaceous (around 400 ppmv), resulting in a decrease in global mean annual continental temperatures from about 20°C to 10°C. Silicate weathering feedback and paleogeography both act to force the Earth system toward a dry and hot world reaching its optimum over the last 260 Myr during the Middle-Late Triassic. In the super continent case, given the persistent aridity, the model generates high CO_2 values to produce very warm continental temperatures. Conversely, in the fragmented case, the runoff becomes the most important contributor to the silicate weathering rate, hence producing a CO_2 drawdown and a fall in continental temperatures. Finally, another unexpected outcome is the pronounced fluctuation in carbonate accumulation simulated by the model in response to the Pangea breakup. These fluctuations are driven by changes in continental carbonate weathering flux. Accounting for the fluctuations in area available for carbonate platforms, the simulated

ratio of carbonate deposition between neritic and deep sea environments is in better agreement with available data.

Components: 11,656 words, 9 figures, 2 tables.

Keywords: carbon cycle; climate; modeling; Pangea; Mesozoic; CO_2.

Index Terms: 0428 Biogeosciences: Carbon cycling (4806); 1036 Geochemistry: Magma chamber processes (3618); 1030 Geochemistry: Geochemical cycles (0330).

Received 16 February 2006; **Revised** 11 July 2006; **Accepted** 8 September 2006; **Published** 22 November 2006.

Donnadieu, Y., Y. Goddéris, R. Pierrehumbert, G. Dromart, F. Fluteau, and R. Jacob (2006), A GEOCLIM simulation of climatic and biogeochemical consequences of Pangea breakup, *Geochem. Geophys. Geosyst.*, *7*, Q11019, doi:10.1029/2006GC001278.

1. Introduction

[2] On timescales longer than about 100,000 years, the carbon cycle is controlled by exchanges between igneous and sedimentary rocks and the atmosphere and ocean. Two slow processes dominate the long-term evolution of CO_2 levels: the CO_2 sink driven by the chemical weathering of silicate (as long as the ocean is oversaturated with respect to carbonates), and the CO_2 source through degassing caused by metamorphic and volcanic processes. The geological evolution of the carbon cycle is a succession of perturbations forcing the carbon cycle to fluctuate around a mean steady state, itself fully determined by the balance between degassing and silicate weathering. Corresponding to this mean steady state is a mean atmospheric CO_2 content, which is the mean background value toward which the geochemical and climatic systems tend to converge when the system is relaxing, with no perturbations applied [*François and Goddéris*, 1998]. In this contribution, we focus our attention on the calculation of these steady state CO_2 concentrations (and associated climate) for time slices covering the Pangea breakup (from 250 to 65 Ma). Our approach also considers potential impacts of the paleogeography on the marine carbonate precipitation rate. Indeed, in our model, the climate induced by paleogeography setting affects the rate of continental carbonate weathering.

[3] The two climatic factors affecting the rate of continental silicate weathering are the air temperature and the continental runoff [*Brady*, 1991; *Brady and Carroll*, 1994; *Dessert et al.*, 2001, 2003; *Oliva et al.*, 2003; *Walker et al.*, 1981]. Both of these factors are strongly linked to atmospheric PCO_2 via the greenhouse effect. On the basis of the existence of this relationship, *Walker et al.* [1981] formulated a negative feedback mechanism which could stabilize the Earth's climate at the geological timescale. The essence of the mechanism is that accumulation of CO_2 in the atmosphere would be compensated by an increase in its removal through silicate weathering under enhanced greenhouse conditions, given that air temperature and continental runoff both increase with PCO_2; the PCO_2 increase would halt at the point where the silicate weathering rate balances the rate of input by outgassing. Although such mathematical relationships may seem to neglect the role of mechanical erosion on chemical weathering [*Millot et al.*, 2002], mechanical erosion is nevertheless included within these parametric laws, either within the value of the activation energy or within the proportionality constant used. Indeed, the most recent parametric laws linking chemical weathering to climate [*Dessert et al.*, 2003; *Oliva et al.*, 2003] are based on a compilation of chemical weathering rates for more than 100 monolithological catchments where mechanical erosion is active. By applying these weathering laws to the geological past, we hypothesize that the link between mechanical erosion and chemical weathering has remained the same. Of course, such an assertion deserves inspection for future work.

[4] Over the years since *Walker et al.* [1981] appeared, much work has been directed at reconstructing atmospheric CO_2 concentration through Phanerozoic times either by relying on numerical modeling or by using various proxies. The former method is mainly based on the GEOCARB model built by R.A. Berner and colleagues [*Berner*, 1991; *Berner and Kothavala*, 2001], and similar models [*Wallman*, 2001], that calculate a globally averaged CO_2 consumption by weathering of continental

Ca-Mg silicates as a function of global mean air temperature and runoff, and of various key parameters (such as the geological history of the land area, or the emergence of gymnosperms or angiosperms). Global mean air temperature is calculated as a function of the solar constant and partial atmospheric CO_2 pressure. Global continental runoff is assumed at the first order to increase by 4% per degree in global mean air temperature. While such models reproduce an atmospheric CO_2 evolution in reasonably good agreement with the warm and cool mode of the climate system (as exemplified by *Crowley and Berner* [2001]), they use a 0-dimensional approach to estimate the main factors controlling the strength of the negative feedback described above, i.e., the land temperature and the river runoff. However, the relationship linking the global runoff to the temperature [*Labat et al.*, 2004] has probably changed over the Earth history in response to changes in the land-ocean configuration. In addition, when using such a 0-D approach, the influence of regional climatic patterns such as monsoons or the presence of large arid regions cannot be accounted for in the calculation of the CO_2 consumption. For these reasons, we decided to revisit the atmospheric CO_2 evolution at geologic timescales using a different method, one in which the climate and the water cycle are explicitly simulated by a general circulation model (GCM).

[5] In a previous paper, we have developed such a climate-carbon model, called GEOCLIM [*Donnadieu et al.*, 2004a, 2004b; *Goddéris et al.*, 2005], characterized by an explicit 2-D representation of the weathering fluxes. This new tool has been useful in helping us to understand the fundamental process responsible for Neoproterozoic glaciations. We have shown that the Rodinia breakup triggered a cold climate throughout the Neoproterozoic by lowering the atmospheric CO_2 level by 1300 ppmv. This CO_2 decrease is the result of an increase in weathering fluxes due to the enhancement of the equatorial runoff following the breakup of the supercontinent. The question of whether the tectonics could have likewise influenced the atmospheric CO_2 level during the Pangea breakup (250–65 Ma) is a fundamental one that deserves inspection. Our objective is to isolate and to quantify the effect of changing geography over the Mesozoic on the atmospheric CO_2 content. The idea is to examine the potential magnitude of continental drift control on the long-term atmospheric CO_2 and climate variations over the Mesozoic by focusing on 7 typical time slices during the Pangea breakup process.

2. Models and Experiments

2.1. General Design of the GEOCLIM Model

[6] Rather than use the CLIMBER-2 climate model [*Petoukhov et al.*, 2000] as done in previous works [*Donnadieu et al.*, 2004a, 2004b; *Goddéris et al.*, 2005] to provide the climatic variables, air temperature and continental runoff required by the COMBINE model to calculate silicate weathering, we chose to use the general circulation model FOAM1.5 [*Jacob*, 1997]. Indeed, the crude resolution of the CLIMBER-2 model (10°lat $\times$ 50°long) is not adequate for the subtle changes in continental configuration we want to investigate. The atmospheric component of FOAM is a parallelized version of NCAR's Community Climate Model 2 (CCM2) with the upgraded radiative and hydrologic physics incorporated in CCM3 v. 3.2. The atmosphere runs at R15 spectral resolution (4.5° $\times$ 7.5°) with 18 levels. The ocean component (OM3) is a z-coordinate ocean model that has been optimized for performance and scalability on parallel computers. OM3 contains 24 vertical layers, a 128 $\times$ 128 grid (1.4° $\times$ 2.8°) and uses simple second order differencing and a fully explicit time step scheme for the barotropic and baroclinic modes. The ocean and atmospheric models are linked by a coupler, which implements the land and sea ice models and calculates and interpolates the fluxes of heat and momentum between the atmosphere and ocean models [*Jacob*, 1997]. FOAM successfully simulates many aspects of the present-day climate and compares well with other contemporary medium-resolution climate models; it has also been used previously to investigate Cretaceous and Neoproterozoic climates [*Donnadieu et al.*, 2006; *Poulsen*, 2003; *Poulsen et al.*, 2001, 2002]. For this study, we use FOAM in mixed-layer mode, i.e., the atmospheric model is linked to a 50-meter mixed-layer ocean, which parameterizes heat transport through diffusion, mainly for computation time considerations (each GEOCLIM simulation requires up to 12 GCM simulations, as described below).

[7] A full coupling between COMBINE and FOAM cannot be achieved owing to excessive computation times. Hence we adopt an indirect coupling that employs look-up tables from a catalog of simulations. For a given paleogeography we

Table 1. Main Results of the GEOCLIM Reference Simulations for the Selected Time Slices[a]

Time Slice	Solar Cst	PCO_2	Air Global T	Air Continental T	Global Annual Runoff
Late Permian	−2.5% (−1)	2420 ppmv (1465)	21.4 C (21.14)	19.1 C (18.7)	28.9 cm/yr (28.9)
Early Triassic	−2.5%	3620 ppmv	21.5 C	18.8 C	25.4 cm/yr
Middle-Late Triassic	−1.8% (−1)	3125 ppmv (2500)	23.1 C (22.7)	22.5 C (21.9)	23.5 cm/yr (23.5)
Late Early Jurassic	−1.8% (−1)	692 ppmv (482)	18.4 (18.6)	17.1 (17.3)	27.9 cm/yr (27.45)
Early Cretaceous	−1.4% (−1)	529 ppmv (438)	17.02 C (16.7)	12.59 C (12.15)	32.7 cm/yr (33.2)
Mid Cretaceous	−1.%	403 ppmv	16.85 C	8.9 C	42.4 cm/yr
Late Cretaceous	−0.8% (−1)	261 ppmv (305)	16.6 C	10.2 C	34.9 cm/yr

[a] Numbers in parentheses correspond to the results of simulations where the solar constant is held constant at 99% of its present-day value.

run a suite of FOAM experiments (30 years for each to reach the steady state) in which the only varying factor is the atmospheric CO_2. The tested values of atmospheric CO_2 range from 4200 to 200 ppm, a range which covers all plausible atmospheric CO_2 content for the Mesozoic time period [*Royer*, 2003; *Royer et al.*, 2001]. Then, we assume a linear behavior in between each climatic simulation and thus, by doing a linear interpolation, we obtain the climatic variables of interest (temperature and runoff) for any PCO_2 on the 48 × 40 grid. These climatic parameters allow the calculation of the weathering rates within the 1920 grid elements using weathering laws linking climatic factors (temperature and runoff) to CO_2 consumption through silicate weathering. Fixing the CO_2 degassing to a given constant value, the numerical feedback loop between FOAM and COMBINE is run until a steady state PCO_2 is reached. Each continental configuration is thus finally characterized by a steady state atmospheric PCO_2.

2.2. Climatic Simulations

[8] We ran FOAM for 7 distinct time periods ranging from the Late Permian (260 Ma) to the Late Cretaceous (68 Ma) (Table 1). The land-ocean distributions for the model experiments are derived from a synthesis of paleomagnetic data, hot spot tracks and geologic constraints [*Besse and Courtillot*, 2002; *Dercourt et al.*, 1993]. Shared boundary conditions for all continental configurations are (1) surface types are set to average model surface characteristics (i.e., deciduous forest) and (2) the Earth's orbit around the Sun is circular (eccentricity = 0) and the Earth's obliquity is 23.5° (this setting leads to an equal annual insolation for both hemispheres). Solar luminosity is assumed to evolve through time according to the stellar evolution models [from 2.5% reduction in the Permian to 0.6% in the Maastrichtian [*Gough*, 1981]. Another set of experiments has been done at a solar constant fixed at a constant 1% reduction relative to the present value for all time slices, to isolate the influence of the evolving land-ocean configurations without taking account of the interactions between changes in solar constant and the atmospheric CO_2 [*Walker et al.*, 1981].

2.3. Geochemical Simulations

[9] The COMBINE model has been upgraded since its original version [*Goddéris and Joachimski*, 2004]. The geometry of the ocean has been changed, and the model now includes 9 oceanic boxes divided into, 2 high latitude oceans (each including a photic zone and a deep ocean reservoirs), a low to mid latitude ocean (with a photic zone, thermocline and deep oceanic reservoirs) and an epicontinental sea (with a photic zone and a deep epicontinental reservoirs), and one box for the atmosphere. The only two parameters eventually defining the steady state PCO_2 are the volcanic CO_2 degassing, and the total continental silicate weathering (sum of silicate weathering on each grid cell). An exhaustive description of the processes described in the COMBINE model is thus not of primary importance for the present study but is given by *Goddéris and Joachimski* [2004].

[10] Total CO_2 consumption through weathering of granitic lithologies is taken from *Oliva et al.* [2003], based on a data compilation for about 100 small granitic catchments:

$$F_{silw} = \sum_{i=1}^{n_{pixel}} k_{silw} \cdot run(i) \cdot area(i) \cdot \exp\left[\frac{E_a^{silw}}{R}\left(\frac{1}{T(i)} - \frac{1}{T_0}\right)\right] \quad (1)$$

where F_{silw} is the total atmospheric CO_2 consumption flux through granitic weathering, R is the perfect gas constant, E_a^{silw} is the apparent activation energy of 48200 J/mol, $area(i)$ is the surface of the continental grid cell, and n_{pixel} is the number of continental grid cells. $T(i)$ and $run(i)$ are respec-

tively the mean annual ground air temperature and the mean annual runoff for the grid cell i.

[11] Weathering of basaltic lithologies is calculated following *Dessert et al.* [2001]:

$$F_{basw} = \sum_{i=1}^{n_{pixel}} k_{basw} \cdot run(i) \cdot area(i) \cdot \exp\left[\frac{E_a^{basw}}{R}\left(\frac{1}{T(i)} - \frac{1}{T_0}\right)\right] \quad (2)$$

where F_{basw} is the total atmospheric CO_2 consumption flux through basaltic weathering. E_a^{basw} is fixed at 42300 J/mol. The calibration of the k_{basw} and the k_{silw} was performed using a present-day control FOAM simulation, and assuming that 30% of the total CO_2 consumption through silicate weathering is due to basalt weathering [*Dessert et al.*, 2003]. Furthermore, total CO_2 consumption through silicate weathering was fixed to 13.6×10^{12} mol/year to match the *Gaillardet et al.* [1999] (updated by *Dessert et al.* [2003]) estimation for the present-day.

[12] Regarding the volcanic CO_2 degassing, no clear consensus exists between the various reconstructions of the degassing flux through the geological past. For instance, recent reevaluations of the ridge production since 180 Ma (using two different methods) suggest a roughly constant degassing rate since the middle Jurassic [*Cogné and Humler*, 2004; *Rowley*, 2002], in complete disagreement with previous reconstruction [*Engebretson et al.*, 1992; *Gaffin*, 1987]. These uncertainties strongly influence the validity of the 0-D models, since CO_2 degassing is the first order driver of the global carbon cycle in such model. Because our aim is to define the impact of the paleogeography on the long-term atmospheric CO_2, we keep the degassing flux at its modern value (6.8×10^{12} moles of carbon per year, which is the value required to balance the global consumption through the weathering of silicate lithologies) for the suite of experiments.

[13] Because continental climate evolves during the breakup of the Pangea supercontinent, changes in the transfer of phosphorus from the continents toward the ocean are expected. Hence oceanic productivity (including calcareous nanoplankton productivity) and possibly organic carbon burial would have varied as well. Modeling phosphorus weathering at the global scale is a difficult task, mainly because the behavior of phosphorus is rather distinct from the behavior of major cations in weathering environments. Most of the phosphorus appears to be released on the geological timescale through the dissolution of apatite present as trace mineral in most silicate lithologies but also in carbonate lithologies [*Guidry and MacKenzie*, 2000; *Guidry and Mackenzie*, 2003]. Here, we modify the original COMBINE code [*Goddéris and Joachimski*, 2004] to include the formalism from *Guidry and MacKenzie* [2000]. Total release of dissolved phosphorus to the rivers through weathering processes is now modeled as follows:

$$F_{pw} = \sum_{i=1}^{n_{pixel}} k_{pw} \cdot run(i) \cdot area(i) \cdot \exp\left[\frac{E_a^{pw}}{R \cdot T(i)}\right] \cdot H_{soil,i}^{0.27} \quad (3)$$

where E_a^{pw} equals 34777 J/mol, k_{pw} is a calibration constant fixed so that P release through weathering equals 45×10^9 mol/yr [*Petsch and Berner*, 1998] under present-day climatic conditions. $H_{soil,i}$ is the proton concentration in soil solution for pixel i. $H_{soil,i}$ is calculated as the proton concentration of a solution equilibrated with the soil PCO_2. Soil PCO_2 depends on the vegetation net primary production, organic carbon content of the soil, moisture, temperature and soil characteristics. None of these parameters can be estimated precisely for the geological past. We adopt a simple parameterization assuming first that the maximum soil PCO_2 is a function of runoff, based on the relationship between net primary productivity and annual mean air temperature for modern ecosystems [*Lieth*, 1984]:

$$PCO_2^{soil}(\max) = 1 + 0.30 \cdot run(i)^{0.8} \quad (4)$$

where $run(i)$ is expressed in cm/yr, and PCO_2 in PAL. Then this value is weighted by an air temperature factor, assuming higher soil PCO_2 under warmer climate due to enhanced soil organic carbon degradation [*Gwiazda and Broecker*, 1994]:

$$PCO_2^{soil} = PCO_2^{atm} + \frac{PCO_2^{soil}(\max)}{1 + \exp(1.315 - 0.119 \cdot T(i))} \quad (5)$$

where $T(i)$ is expressed in Celsius and PCO_2^{atm} is the atmospheric pressure in PAL. This doubled dependency of soil CO_2 on climatic parameters ensures low productivity and low soil CO_2 in too arid and/or too cold areas.

[14] The formulation of carbonate weathering F_{cw} was improved in the present version of the COMBINE model. We removed the previous weathering law that assumed a CO_2 consumption

through carbonate weathering proportional to the square root of runoff, and replaced it with a much more physical approach. Calcium concentration $[Ca^{2+}]_{eq}$ within a soil solution in equilibrium with soil CO_2 and carbonate rock is calculated at each time step and for each pixel i, with equilibrium constant made dependent on mean annual air temperature itself given by the FOAM GCM. Air temperature dependence of the solubility product of calcite is taken from *Usdowski* [1980].

$$F_{cw} = \sum_{i=1}^{n_{pixel}} k_{cw} \cdot run(i) \cdot area(i) \cdot \left[Ca^{2+}\right]_{eq} \quad (6)$$

k_{cw} is a calibration constant so that the total consumption of CO_2 through carbonate weathering matches 23.0×10^{12} moles/yr. This value has been fixed so that total supply of alkalinity (silicate + carbonate weathering) to the oceans reaches about 60×10^{12} eq/yr, corresponding to a total carbonate deposition at steady state of 30×10^{12} moles/yr [*Milliman*, 1993].

[15] The relative proportions of silicate (and among them of granitic and basaltic lithologies) and carbonate outcrops is assumed to be the same in each grid cell because of the current lack of precise lithological control. These relative proportions are not expressed in terms of relative area, but rather in terms of contribution of each lithology to the CO_2 consumption flux, so that total silicate weathering reaches 13.6×10^{12} moles/yr (with 30% due to basaltic weathering), and carbonate weathering 23×10^{12} moles/yr. This requires that under the same climatic conditions (in terms of mean annual air temperature and continental runoff), the contribution to the CO_2 sink per m^2 through granitic or basaltic and carbonate weathering is identical for each continental grid cell.

[16] Carbonate deposition is modeled as the sum of two fluxes: the accumulation of neritic carbonates on the shelf floor, and the accumulation of pelagic carbonates. Note that total removal of oceanic alkalinity through carbonate accumulation will be the sum of the alkalinity flux from continental silicate and carbonate rocks weathering for all simulated periods. Although this equality between destruction and production of alkalinity is not formally prescribed in the model, the saturation state of the ocean will adapt until this equality is reached. The total carbonate deposition flux is thus totally independent of the exact kinetics of deposition assumed, but is dependent on the partition between neritic and pelagic production.

[17] The neritic term $F_{neritic}$ is calculated as follows [*Goddéris and Joachimski*, 2004]:

$$F_{neritic} = k_{cr} \cdot A_{platform} \cdot (\Omega_{ara} - 1)^{1.7} \quad (7)$$

where $A_{platform}$ is the shelf area occupied by platform carbonate, Ω_{ara} is the model aragonite solubility ratio and k_{cr} a calibration constant. The power 1.7 is taken from *Opdyke and Wilkinson* [1993]. We assume a dependence on the solubility ratio of aragonite instead of calcite for all time slice simulations. Future refinements of the model should account for the shift from aragonitic to calcitic production for past periods [*Hardie*, 1996; *Sandberg*, 1983]. The total shelf area available for carbonate platform $A_{platform}$ is assumed to have changed through time according to *Walker et al.* [2002]. This area was roughly 15 to 20 times larger for each simulated time slice, as compared to the present-day surface.

[18] The accumulation rate of pelagic carbonates is estimated from the calculated carbonate saturation state of the ocean and lysocline depth, and from the ocean hypsometry (itself assumed constant below 100 m depth at its present-day configuration in the absence of reliable reconstructions). The complete carbonate speciation is thus calculated for each oceanic box. The partition between deep sea and neritic carbonate is based on the estimation of the present-day (mean glacial-interglacial) deep sea carbonate accumulation of 8.7×10^{12} moles/yr [*Catubig et al.*, 1998], the remaining 22×10^{12} moles/yr being shelfal. This partition is obtained for present-day conditions by adjusting the calibration constant k_{cr}. This constant is then kept unchanged for all past simulations.

[19] Finally, when calcareous nanoplankton production is allowed, we simply assume that 30% of the calculated primary productivity in the surface reservoir of interest is mobilized as a carbonate mineral production, if the waters are oversaturated with respect to aragonite ($\Omega_{ara} > 1.7$). No carbonate production occurs when Ω_{ara} is below 1.5. Between these two values, the fraction of carbonate in the primary production is a linear function of Ω_{ara} [*François et al.*, 1993]. This calculated carbonate production is modulated by the history of calcareous nanoplankton emergence. The first occurrence of calcareous nanoplankton in the pelagic environment is dated around the Triassic-Jurassic boundary. It was most probably first restricted to shelf environments [*Bown et al.*, 1988; *Kuznetsova*, 2003; *Roth*, 1986]. In the GEOCLIM simulations, we thus force calcareous nanoplankton productivity

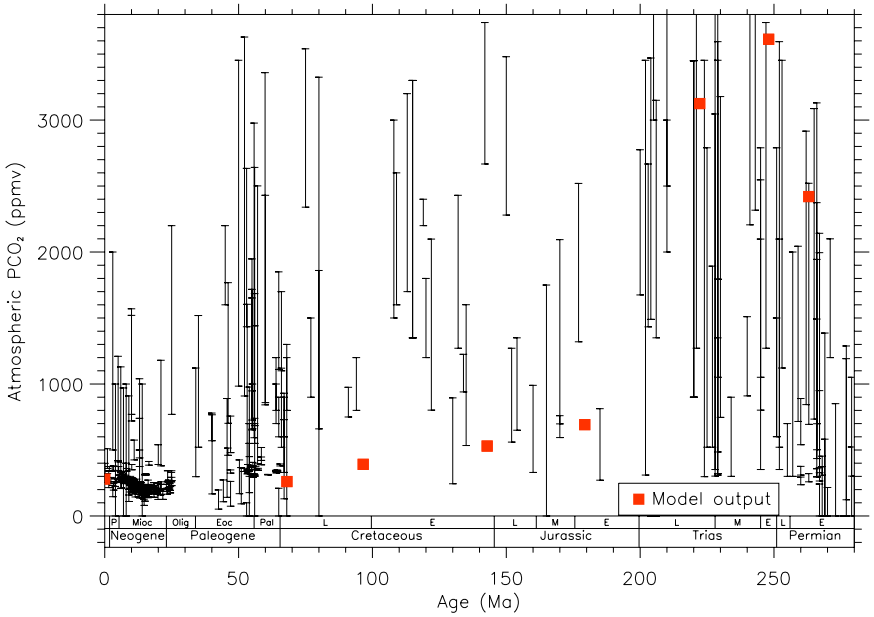

Figure 1. Evolution of atmospheric CO_2 through the Mesozoic. Bars represent atmospheric CO_2 estimates (min-max values) coming from the data sets built by *Royer* [2004] and available online at http://www.geosociety.org/pubs/ft2004.htm. The squares represent the modeled atmospheric CO_2 in the reference run under boundary conditions fully described in the text.

at a very low level for the two first time slices by multiplying the calculated calcareous nanoplankton production by a factor of 10^{-2} (late Permian and early Triassic), then restrict this production to the shelf environments (epicontinental sea surface reservoir) for the Middle-Late Triassic and late Early Jurassic, while the early, middle and late Cretaceous are characterized by an efficient calcareous nanoplankton production (similar to the present-day one) in shelf and open ocean environments.

3. Consequences of the Pangea Breakup on the Global Carbon Cycle

[20] The reference runs were all performed at constant degassing rate of the solid Earth, evolving solar luminosity and fluctuating area for neritic carbonate deposition. Going from the Late Permian to the Late Cretaceous, our results show that calculated atmospheric CO_2 pressure is at a zenith during the Early Triassic (3620 ppmv) and decreases throughout the Mesozoic to reach 261 ppmv during the Late Cretaceous (Table 1 and Figure 1). Paleolocation of continents turns out to be a major controlling factor of the CO_2 over the Mesozoic era. Indeed, when assuming a fixed solar constant 1% dimmer than present, the steady state atmospheric CO_2 pressure is generally decreased. However, the general pattern of the simulated CO_2 curve is nearly similar, underscoring the fundamental importance of the paleogeography in controlling atmospheric CO_2 when outgassing is held constant.

[21] We now consider the mechanisms whereby paleogeography influences the global simulated climate and in turn the weathering pattern. As shown by *Gibbs et al.* [1999], from a global point of view, the breakup of Pangea causes a transition from a generally dry climatic regime during the Triassic to a wetter one during the Cretaceous (continental runoff strongly increases by about 46% from the Early Permian to the Mid Cretaceous in our runs). In the same time, global and continental air temperature decreases by about 6 and 10°C, respectively (Table 1). Hence, when plotting the global mean runoff versus mean air temperature for each geological period, a general scenario emerges (Figure 2). Silicate weathering feedback and paleogeography both act to force the Earth system toward a dry and hot world reaching its optimum over the last 260 Myr during the Middle-Late Triassic. The other pole in our T-R diagram corresponds to the coldest and wettest world which characterizes the Cretaceous geographies with the optimum attained during the Mid-Cretaceous.

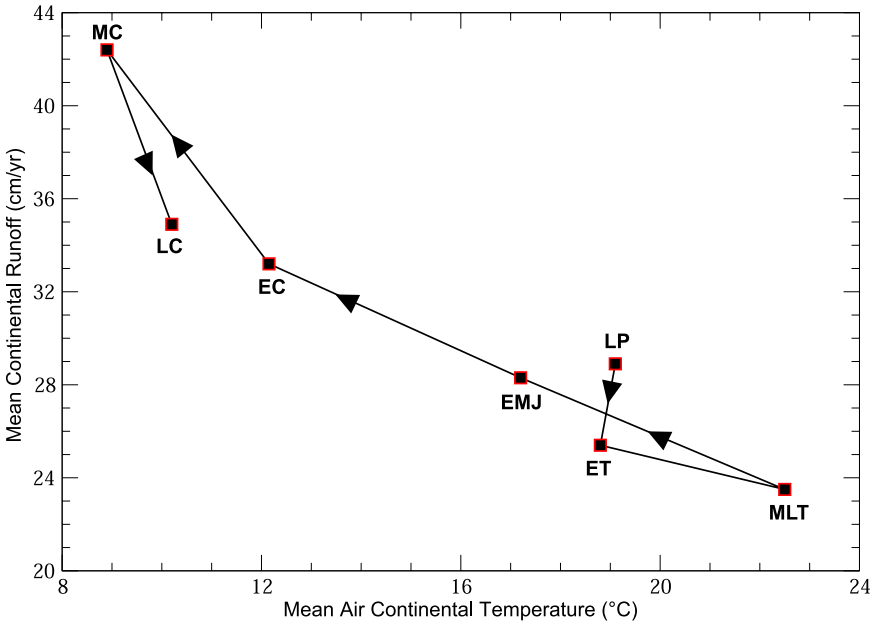

Figure 2. Global annual average of the continental air temperature and runoff as simulated by FOAM at the steady state atmospheric CO_2 estimated by GEOCLIM (see Table 1) for the seven geographies (LP for Late Permian, ET for Early Triassic, MLT for Middle Late Triassic, EMJ for Early Middle Jurassic, EC for Early Cretaceous, MC for Middle Cretaceous, and LC for Late Cretaceous). In FOAM, surface runoff is generated whenever the upper soil layer infiltration capacity is exceeded. This depends on local precipitation minus evaporation rates, preexisting soil wetness, and the specified soil grain size. Subsurface drainage occurs from the base of the lowermost soil layer, which we assume would quickly reach a stream or river (furthermore, it represents the most likely pathway for chemical weathering products).

Explaining this pattern is straightforward. In order to reach the same value for the silicate weathering flux in between each run once steady state is reached (because solid Earth degassing is held constant), there is an interplay between the runoff and the temperature that controls the weathering flux. In the super continent case, given the high aridity owing to extreme continentality, the model generates high CO_2 values to produce the very warm continental temperatures needed to produce the necessary amount of silicate weathering an a low-runoff environment. Conversely, during times of dispersed continents, the runoff becomes the most important contributor to the silicate weathering rate, causing a CO_2 drawdown and a fall in continental temperatures. Hence, because the total alkalinity production through continental silicate dissolution remains the same from one simulation to the other, the mean global riverine concentration in HCO_3^- coming from silicate dissolution fluctuates, displaying high values during dry periods (the highest concentration is reached during the Middle Late Triassic) and low values during humid periods (the lowest concentration is reached during the Mid Cretaceous). These changes in HCO_3^- concentration inversely compensate changes in global water discharge, i.e., large water discharge occurring during humid period results in a dilution of the HCO_3^- ions.

[22] Before further investigating the behavior of the GEOCLIM model, we would like to draw the attention of the readers to the common unique linear positive runoff-temperature relationship used in most numerical model of the long term carbon cycle [*Berner*, 1991; *Berner and Kothavala*, 2001; *François and Walker*, 1992; *Goddéris et al.*, 2001; *Wallman*, 2001] to simulate the evolution of continental weathering rates over geological timescales. In Figure 3, we have plotted the global runoff against the mean air temperature for various atmospheric CO_2 levels (spanning from 4200 to 200 ppmv) and for each continental configuration. For the purposes of this test, we do not calculate CO_2 using GEOCLIM, but instead prescribe it at various values; global runoff and temperature are estimated by the FOAM climate model. Although the runoff increases approximately linearly with the temperature, changes in continental configuration strongly shift the ordinate at the origin (Table 2).

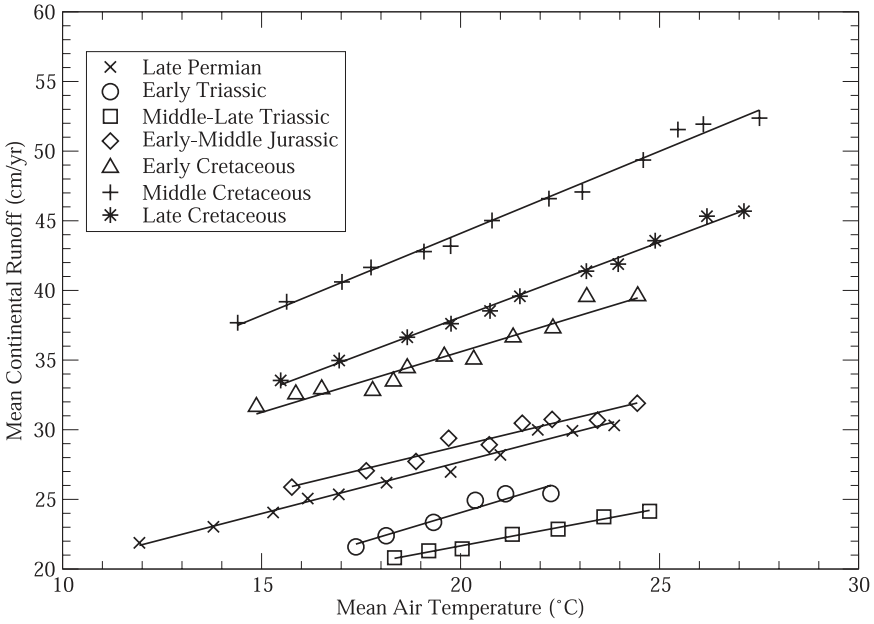

Figure 3. Global annual average runoff against the global mean air temperature. All values have been computed by FOAM for various atmospheric CO_2 levels (see text for a detailed explanation). Each line is a linear fit of the set of values for a given paleogeography. The R^2 values are all greater than 0.98.

The regression coefficient also displays large variations all along the Pangea breakup with a doubling between the Early Middle Triassic and the Mid Cretaceous (Table 2). This clearly demonstrates that a unique positive runoff-temperature relationship may introduce large biases in the estimates of the continental weathering rates. We thus feel that it is of primary importance for future long term carbon cycle to include evolving relationships over time.

[23] In order to better constrain the role played by the introduction of spatial resolution in the GEOCLIM model, we will now take a closer look at the spatial distribution of both terms contributing to the weathering, i.e., the runoff and the air temperature through the exponential factor exp $[E_a/R(1/T - 1/T_0)]$. Indeed, an important nonlinear phenomenon occurs in our model owing to the spatial resolution. For example, the calculated global mean air temperature and runoff are similar for the Late Permian and the late Early Jurassic assuming the same solar constant (Table 1), which should result in the same steady state atmospheric CO_2. However, atmospheric CO_2 is almost divided by 3 between the two time slices (from 1465 to 482 ppmv). This case is interesting as it shows that the globally aggregated approach is not sufficient to represent the silicate weathering feedback.

[24] In order to provide a straightforward illustration of the effect of paleogeography on weathering rate, we use climatic simulations with the same atmospheric CO_2 level (1680 ppmv, i.e., 6 times the preindustrial value) and with the same solar constant to calculate both runoff and temperature weathering factors for each geological period, as well as the total weathering fluxes. Figure 4 shows the evolution of the weathering fluxes by latitudinal band. The late Early Jurassic appears as a period of transition between a world where weathering rates are kept at low level, characteristic of the three preceding time periods (end Permian and

Table 2. Coefficients of the Linear Fit of Runoff Against Mean Global Air Temperature for the Seven Simulated Time Slices[a]

Time Slice	A	B
Late Permian	0.742	12.836
Early Triassic	0.861	6.839
Middle-Late Triassic	0.538	10.908
Late Early Jurassic	0.691	15.042
Early Cretaceous	0.87	18.196
Mid Cretaceous	1.18	20.519
Late Cretaceous	1.075	16.585

[a] The following formulation was used: Runoff (cm/yr) = A × Temperature (°C) + B.

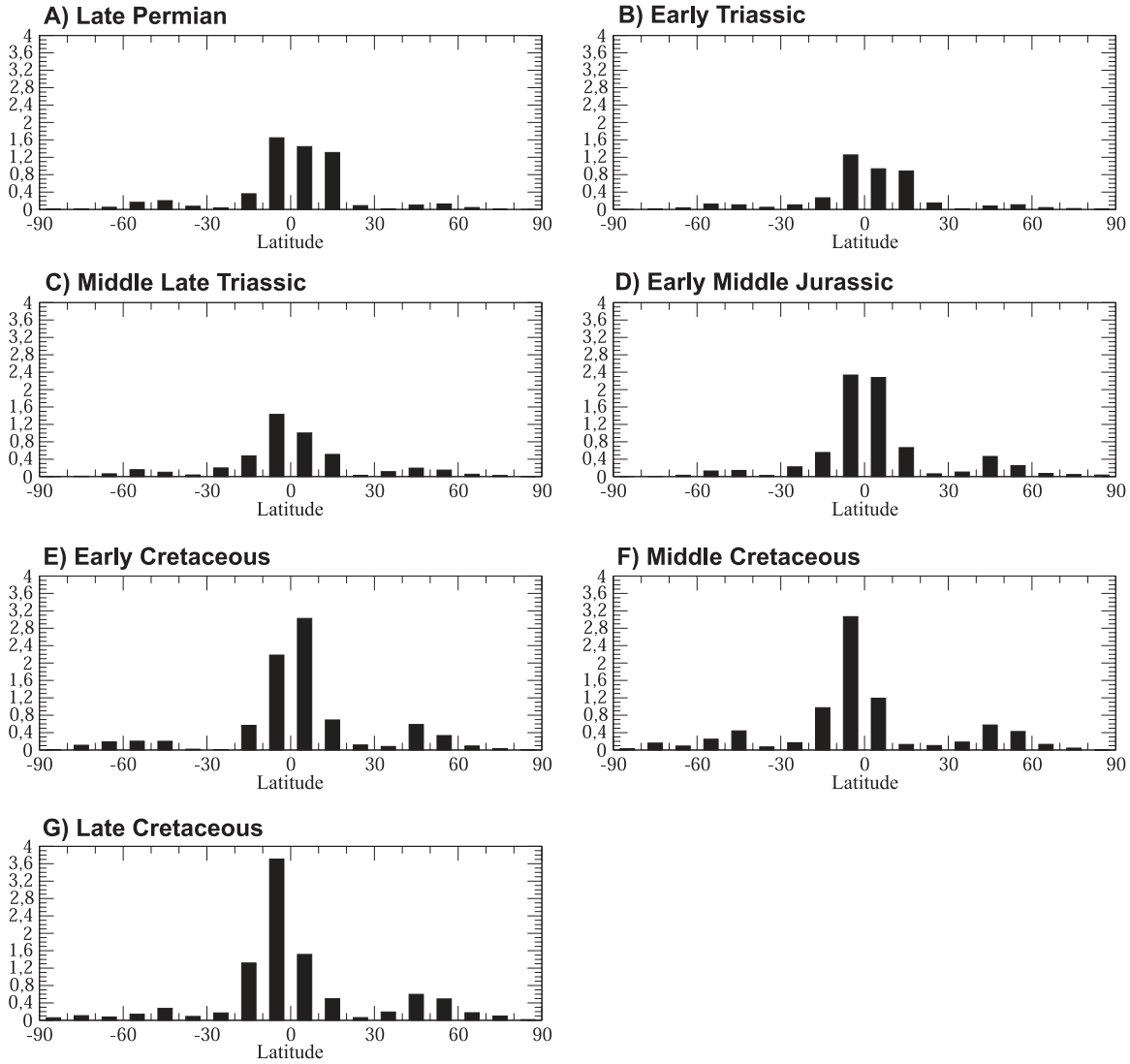

Figure 4. Latitudinal distribution of silicate weathering fluxes. Each bar represents half of the atmospheric CO_2 consumption within a 10° latitude band (units are 10^{12} mol/yr). All climate simulations have been run at a −1% solar constant and at a PCO_2 of 1680 ppm (6x PAL) intermediate between the seven simulated time slices.

Triassic worlds), and the Cretaceous world characterized by high weathering rates.

[25] The increase in atmospheric CO_2 between the Late Permian and the Triassic geographies seen in our reference simulations (Figure 1) (with variable solar constant, but the same feature is observed with a constant solar constant) is explained by the decrease of the weathering flux in the equatorial area. Figure 5 and Figure 6 show that the decrease is more related to changes in runoff (equatorial area is becoming dryer) rather than to changes in the temperature effect on mineral dissolution.

[26] Regarding the decrease in atmospheric CO_2 between the Late Permian and the late Early Jurassic, a larger equatorial weathering flux appears as a good explanation, though a substantial increase of the input coming from the northern midlatitudes is also observed. Both terms contributing to the weathering display an increase. For the late Permian, most of the equatorial runoff came from the western part of Pangea (the eastern part is significantly dry) whereas for the late Early Jurassic, elevated values of equatorial runoff are more widespread from the East to the West and cover a larger area (Figure 5). Hence it is not a change in global mean runoff but rather a change in the distribution of runoff above a larger continental surface that partly explains the increase in weathering between the two time periods. The heating of

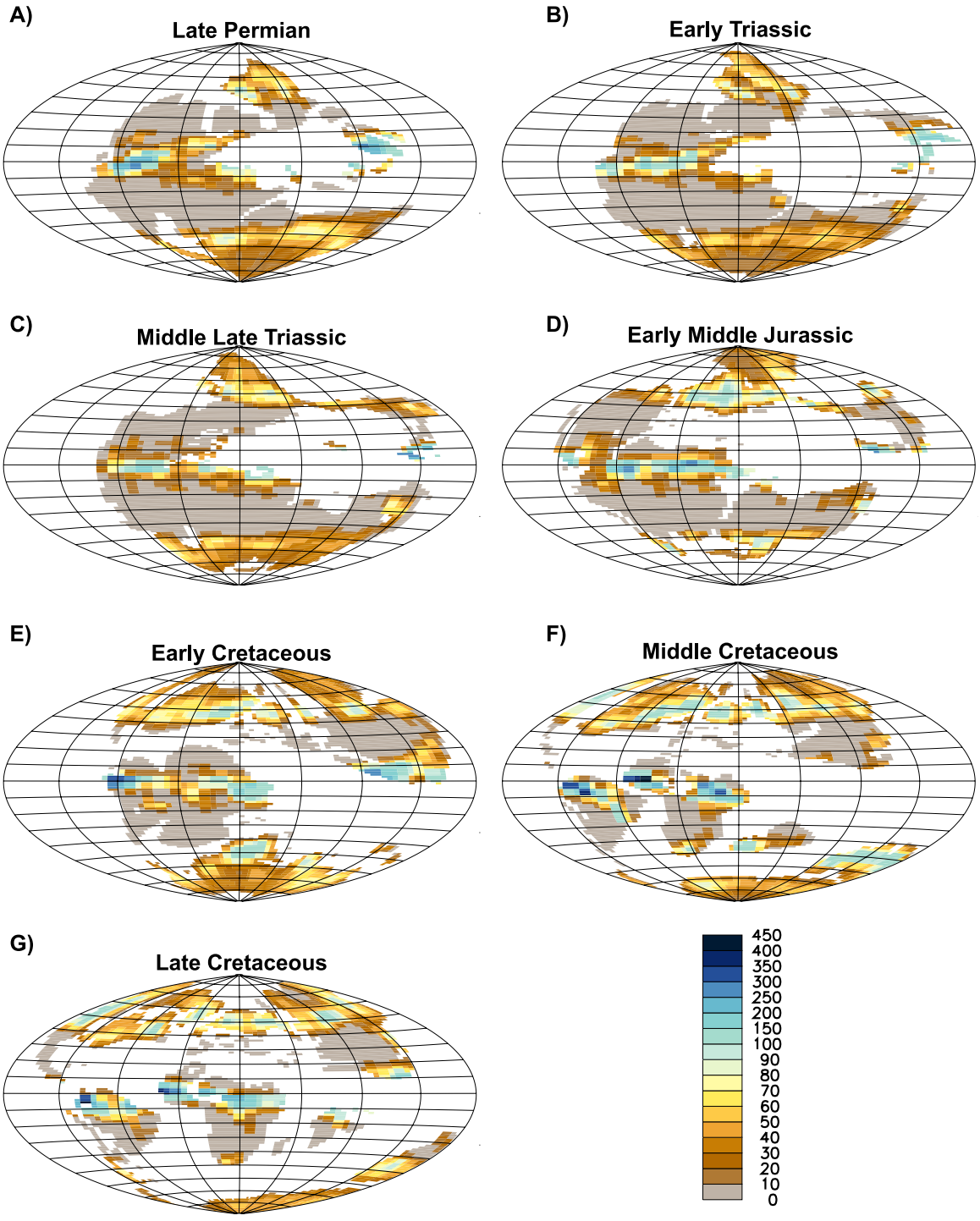

Figure 5. Mean annual runoff (cm/yr) for seven paleogeographies spanning the Mesozoic. All climate simulations have been run at a −1% solar constant and at a PCO_2 of 1680 ppm (6x PAL). Note the uneven shading scale.

the equatorial continental surface during the late Early Jurassic also contributes to the weathering increase (Figure 6). Indeed, the mean continental temperature between −10° and 10° latitude increases by 3.3°C between the two time slices in the model. In fact, the northward drift of the Pangea induces a large decrease in the land area southward of 40°S during the late Early Jurassic. As a consequence, more solar energy is absorbed over the mid to high south latitudes owing to the weaker ocean albedo. This, in turn, warms the southern mid-to-high latitudes and produces a weaker ther-

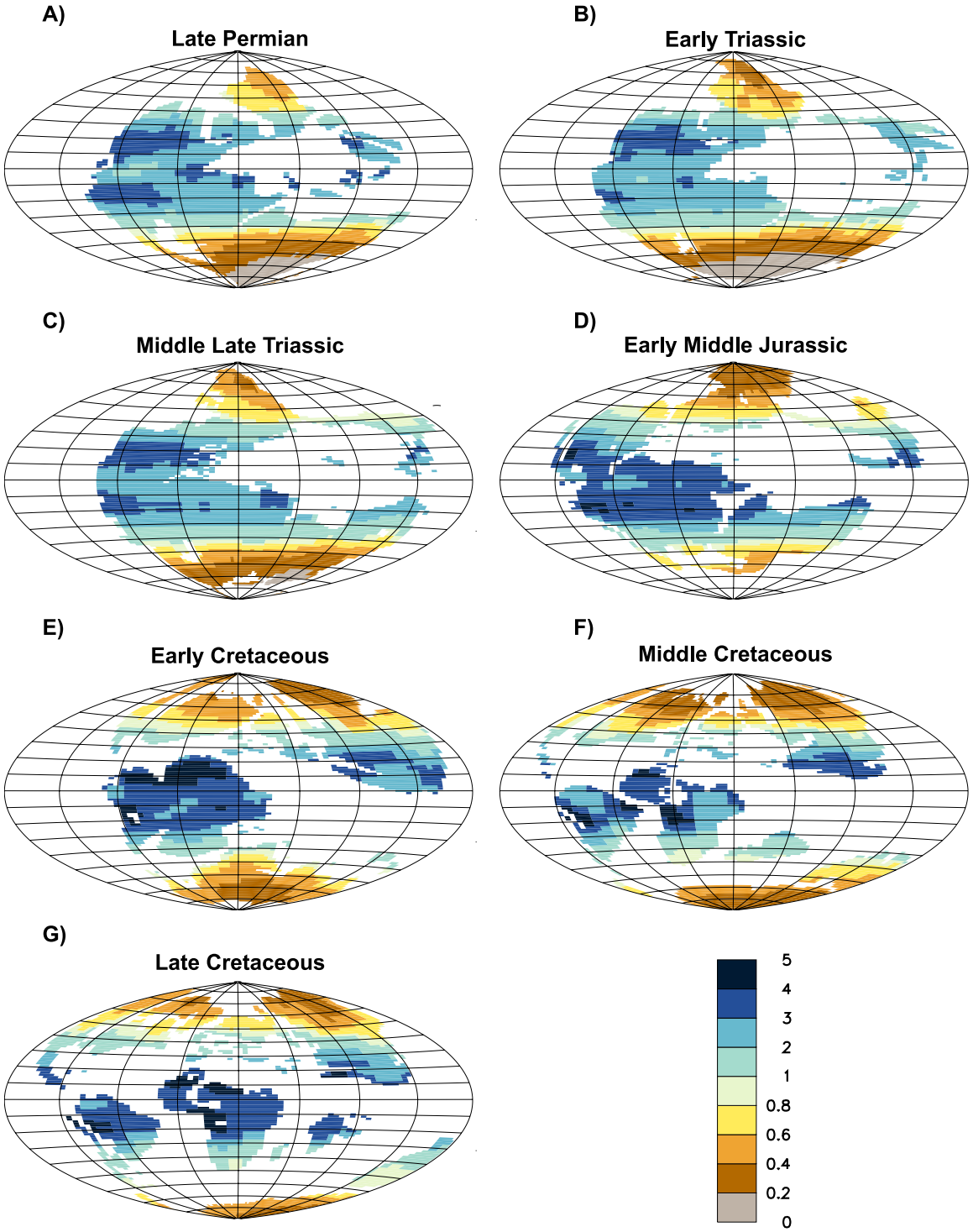

Figure 6. Distribution of the temperature dependence of silicate weathering (exp $[E_a/R(1/T - 1/T_0)]$). All climate simulations have been run at a −1% solar constant and at a PCO_2 of 1680 ppm (6x PAL). Note the uneven shading scale.

mal Equator-South Pole gradient. These changes reduce the zonal heat transport from the Equator to the South Pole and appear responsible for the overheating of the equatorial area though other modifications implying the water vapor feedback probably contribute to the equatorial warming.

[27] The decrease in atmospheric CO_2 simulated between the Jurassic and the Early Cretaceous is

mainly due to changes in continental surface. On one hand, the continental surface within the 0–10°N latitudinal band increases from 23 to 29% of the global surface, on the other hand, the continental surface within the 40–60°N latitudinal band increases from 31 to 44% of the global surface. Both changes generate a larger weathering flux (Figure 4). The runoff over the 0–10°N latitudinal band does not show large variations in between the two time slices and the temperature effect is a little bit larger during the Early Cretaceous (Figures 5 and 6).

[28] Mid Cretaceous and Late Cretaceous record a decrease of continental surface between −10 and 10° latitude when compared to the Early Cretaceous. However, the very large runoff occurring over this area during the Mid Cretaceous and the Late Cretaceous compensates for the loss of surface and maintains a large global weathering flux (Figure 5).

[29] The three Cretaceous climates are the coldest of all the Mesozoic simulations, which is a surprising result given the amount of data suggesting a generally, though not uniformly, warm period [*Stoll and Schrag*, 2000]. However, the calculated Cretaceous continental temperatures are still above the present-day one by 4°C. This is due to the large decrease of the seasonality during the mid-to-late Cretaceous, which is rectified into annual mean changes. These modifications of the seasonality are due to the numerous seaways taking place over the middle latitudes [*Donnadieu et al.*, 2006; *Poulsen et al.*, 1999]. Nonetheless, it does not appear that the generally cool oceanic climates simulated here are compatible with the geological record for the warmer parts of the Cretaceous. Note further that only one forcing is tested here: the paleogeography. The magmatic degassing rate being held constant for each time period simulated in this paper, a data-model comparison of the climate calculated here with paleoclimatic reconstructions is premature, particularly for the Cretaceous period where degassing rate estimates vary significantly. Another possible mechanism affecting Cretaceous CO_2 is the feedback between climate and vegetation cover, which has been neglected in our simulation. Finally, the FOAM simulations suffer from the same shortcoming endemic to all hothouse climate simulations, in that the meridional temperature gradient appears too large for a given global mean temperature. Whatever (presently unknown) process resolves this shortcoming will also affect the weathering rate.

[30] In all simulations, it appears that the response of the silicate weathering rate in the equatorial area is an important driver of the carbon cycle and atmospheric CO_2 (Figures 4–6). However, this might be an artifact of the weathering laws used. High weathering rates sustained for long periods in this warm and humid zone may result in the development of thick soils, which will ultimately limit the consumption of CO_2 through silicate weathering. Though, the reverse argument also holds: thick soils require intense weathering and/or a very long time. Several recent studies show a strong link between mechanical denudation [*Millot et al.*, 2002] or tectonic activity inducing landscape rejuvenation [*von Blanckenburg*, 2005] and chemical weathering of silicates. In the absence of mechanical denudation and/or landscape rejuvenation, chemical weathering in low latitude areas will decrease through time. On the other hand, it will be extremely intense if mechanical denudation is sustained. We implicitly assume here that the weathering law used for silicate rocks can be applied to estimate weathering rates in tropical areas with some kind of a mean denudation rate, higher than the denudation rate of the African craton today, but lower than the extreme denudation rates observed today in Central America, New Zealand or Taiwan [*von Blanckenburg*, 2005].

[31] In summary, continental configurations throughout the breakup of Pangea strongly impacted the climate, which in turn controls the weathering and the atmospheric CO_2. As expected, the interplay between the paleogeography and the carbon cycle results in a large CO_2 consumption between the most assembled case, the Triassic times, and the most dispersed case, the Cretaceous times. But, an unexpected outcome emerged: the moderate northward drifting of the Pangea and the initiation of the breakup (i.e., Pre- to Syn-Rift phases of western Tethyan continental margins) [*Lemoine et al.*, 1986] induce important changes in atmospheric general circulation that lead to a large CO_2 drawdown between the Triassic and the Jurassic.

4. Consequences of the Pangea Breakup on the Oceanic Carbonate Chemistry and Deposition

[32] Fluctuations in the carbonate deposition flux over Earth's history have already been noticed [*Wilkinson and Algeo*, 1989] and are generally thought to be linked to changes in degassing rate

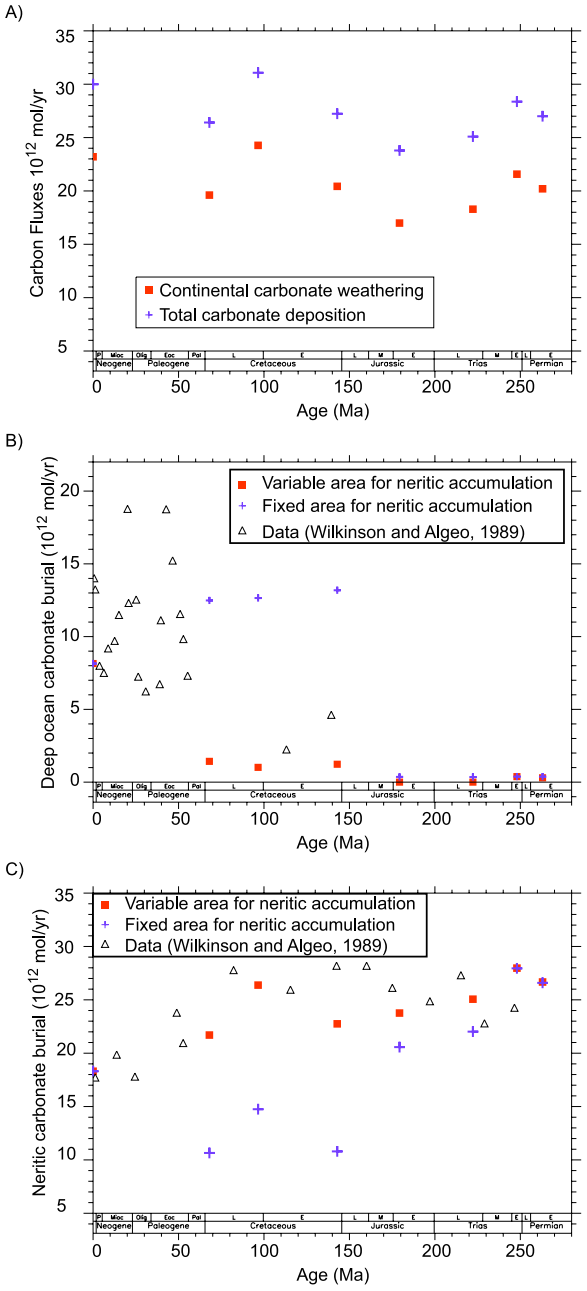

Figure 7. (A) Total carbonate deposition and total continental carbonate weathering for the seven Mesozoic time slices (units are 10^{12} moles of carbon/yr). (b) Carbonate deposition in deep sea environments for two sets of GEOCLIM simulations: shelf area available for neritic carbonate deposition fluctuating through times [*Walker et al.*, 2002] and shelf area available for neritic deposition held at its present-day value (0.6×10^6 km2). The results are compared to available data [*Wilkinson and Algeo*, 1989]. (c) Same results for carbonate accumulation in neritic environments. Note that the original neritic data have been globally shifted upward to match more recent estimation of the present-day deposition rates (see text for details).

(and thus to the global silicate weathering rate) [*Ronov*, 1982]. Here, we explore the effect of the paleogeography on the carbonate weathering rate, which can influence the carbonate deposition rate as well.

4.1. Total Oceanic Carbonate Accumulation

[33] Carbonate deposition is driven by the continental supply of alkalinity from the subaerial weathering of carbonate and silicate rocks. In all simulations, the total supply of alkalinity by silicate weathering is held constant, since it balances exactly the CO_2 degassing rate fixed at a constant value of 6.8×10^{12} moles/yr. Thus any changes in total carbonate accumulation calculated by the model must be related to the fluctuations in continental carbonate weathering, themselves related in fine to the climatic conditions resulting from the balance between silicate weathering and CO_2 degassing. As a consequence, the total carbonate accumulation mimics the time evolution of the carbonate weathering (Figure 7a) with a constant difference in carbonate weathering and deposition fluxes due to the additional supply of alkalinity from silicate weathering, which is evacuated via carbonate deposition. The total carbonate accumulation reaches its maximum during the "middle" Cretaceous ($\sim 31 \times 10^{12}$ moles/year) and displays its lowest value during the late Early Jurassic, with carbonate burial reaching 23.8×10^{12} moles/year (note that the value for the Early Middle Triassic is also particularly low, $\sim 25 \times 10^{12}$ moles/year). Except for these periods, the carbonate accumulation oscillates around 27×10^{12} moles/year. In details, Figure 8 also shows the time evolution of the carbonate weathering fluxes averaged by latitudinal band. Globally, carbonate weathering coming from tropical areas remains an important contributor to the alkalinity flux to the ocean and shows little change except during the Middle Late Triassic where a minimum is simulated. This minimum is also seen in the carbonate production curve. The most interesting point here is to note that the changes in carbonate production are primarily due to changes in carbonate weathering over the mid-to-high latitudes. The decrease in carbonate production during the late Early Jurassic is driven by the dramatic decrease of carbonate weathering in the southern hemisphere linked to the northward drift of Pangea. Indeed, this continental drift induces a significant warming of the southern hemisphere, hence decreasing the dissolution of continental carbonates as the calcite

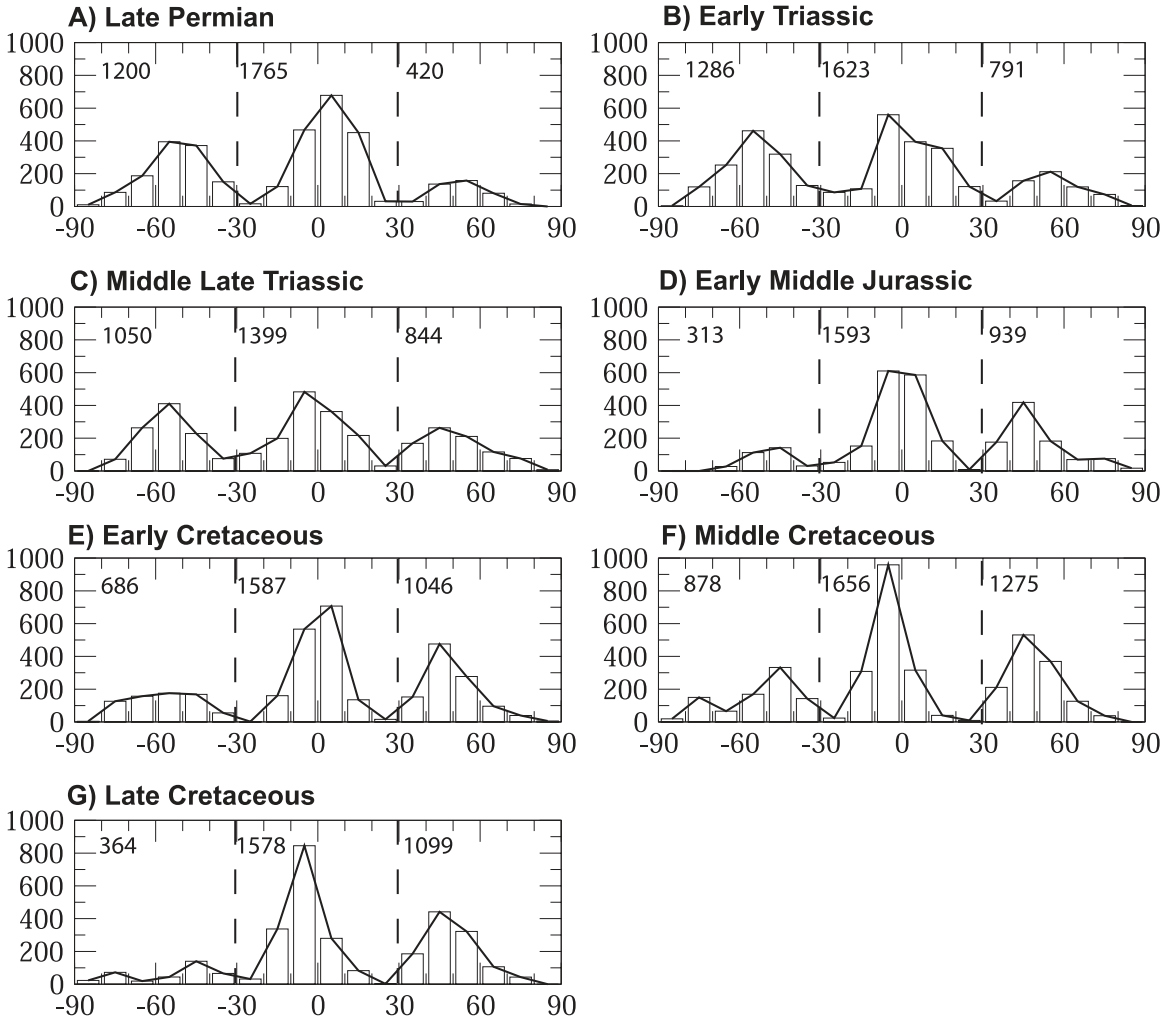

Figure 8. Latitudinal distribution of continental carbonate weathering. Units are 10^{10} mol of carbon/yr. Each bar represents the total flux for a 10° latitude band. All climate simulations have been run at a −1% solar constant and at a PCO_2 of 1680 ppm (6x PAL).

solubility product decreases with an increase in temperature. The increase in carbonate production seen during the Middle Cretaceous is the result of a generally humid climate, particularly over the northern midlatitudes (note the maximum carbonate weathering value of 24×10^{12} moles/year).

[34] For the first time, we show that the breakup of Pangea may have induced large fluctuations in carbonate deposition in response to changes in continental carbonate weathering rate. This result supports recent work emphasizing the role of carbonate cycling in long term carbon cycle evolution [*Ridgwell et al.*, 2003]. Further oscillations would result from fluctuating continental silicate weathering, itself driven by fluctuating solid Earth degassing that are not considered within this work.

4.2. Distribution of Carbonate Accumulation

[35] Deep-sea carbonate burial is maintained at a very low level for all the Mesozoic (Figure 7b). The explanation is twofold. First, the area available for platform carbonate (neritic carbonates) is much larger in the past compared to present-day [*Walker et al.*, 2002]. For instance, this area reaches 13.2×10^6 km^2 in the early Permian simulation [*Walker et al.*, 2002], compared to the 0.6×10^6 km^2 today. Consequently, the saturation state of the epicontinental open surface waters relative to carbonate mineral tends to be low in order to compensate for the increases area in epicontinental surface waters (Ω_{ara}; see equation (5)).

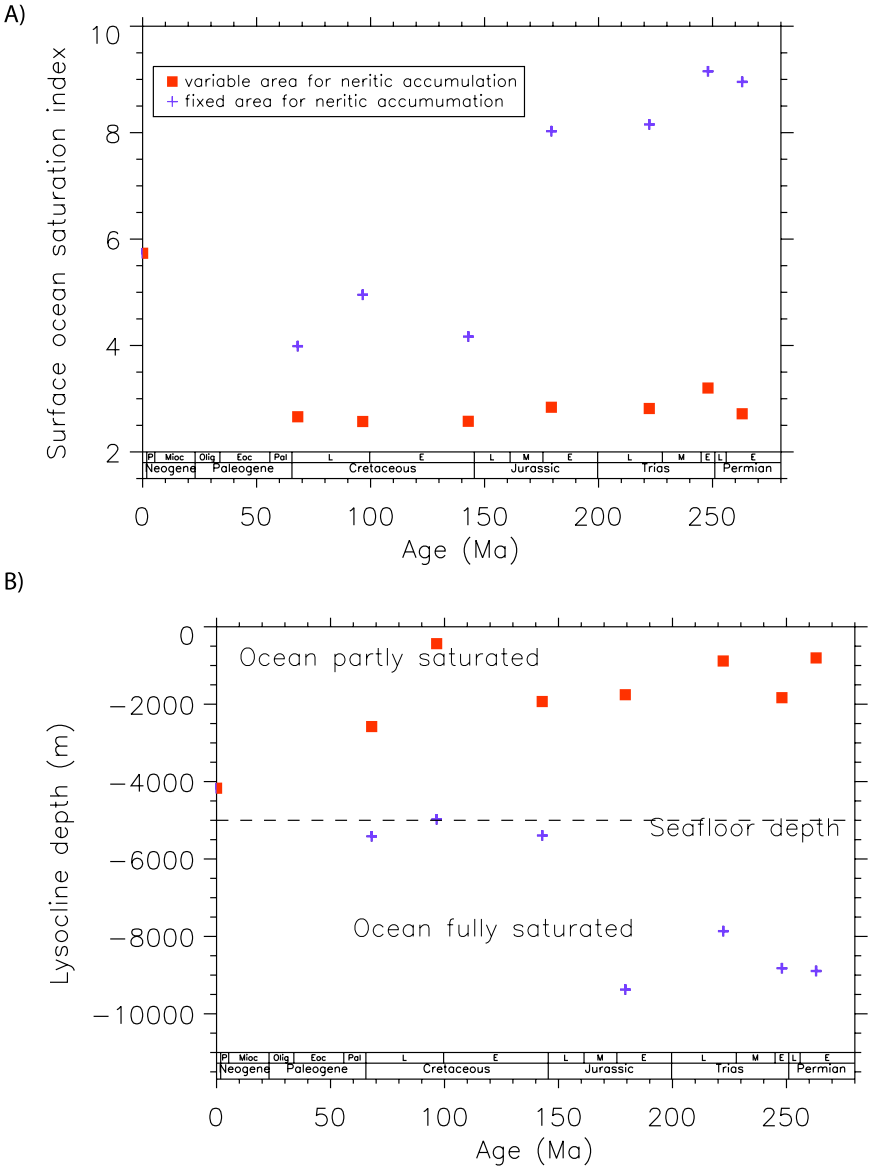

Figure 9. (a) Calculated carbonate oversaturation index for the mid- to low-latitude surface ocean, for two sets of simulations (see Figure 7 caption). (b) Calculated lysocline depth for two sets of GEOCLIM simulations. The calculated lysocline can mathematically deepen below the seafloor in several simulations, particularly when surfaces for neritic accumulation are limited, indicating the degree of supersaturation of the ocean. These below seafloor values show that the ocean is fully saturated with respect to carbonate minerals to a various degree.

Second, the virtual absence of calcareous nannoplankton up to the middle-late Triassic further decreases the carbonate accumulation on the deep seafloor for the three older simulated time slices. On the contrary, neritic deposition displays high values for all the Mesozoic with peak values calculated for the middle Cretaceous ($\sim 26 \times 10^{12}$ moles/yr) (Figure 7c). Calculated lysocline depth displays large fluctuations forced by the Pangea breakup (see below for a detailed discussion of the behavior of the lysocline). The shallowest value is reached during the middle Cretaceous at about 400 m depth (Figure 9b). This calculated shallow lysocline depth for the Mid-Cretaceous is the result of the extreme extension of the carbonate platforms at that time, reaching 14.5×10^6 km^2 (i.e., 25 times the present-day carbonate platform area [*Walker et al.*, 2002]). The multiplication of environmental settings available for neritic deposition forces the model to calculate a severe decrease in the saturation state of the open ocean with respect to carbonate minerals.

[36] These results are rather different compared to a recent model of the ocean chemistry for the last 250 Myr [*Ridgwell*, 2005]. *Ridgwell* [2005] calculates a saturation state of the ocean for the last 250 Myr which is generally equal to or higher than the present-day value. Several major differences appear between the two approaches. First, the Ridgwell model is forced by CO_2 atmospheric pressure reconstructed from available data [*Royer et al.*, 2001], by the weathering rates from the model simulations performed by *Gibbs et al.* [1999], and by Ca^{2+} concentration reconstructed from fluid inclusions analysis [*Horita et al.*, 2002]. On the contrary, GEOCLIM self-consistently calculates these three parameters as a function of the continental configuration, which is the ultimate forcing function together with the solar constant. Second, the evolution of the area available for carbonate platform $A_{platform}$ in the past differs for the GEOCLIM simulations compared to the Ridgwell model. Here, we assume an increase in this surface by up to a factor of 20 [*Walker et al.*, 2002], while *Ridgwell* [2005] calculates an increase by up to a factor of 3 in the past for the shelf area, based on the sea level fluctuations. It should be noted that the factor of about 15 to 20 (fluctuating from one time slice to the other) only applies to the surface occupied by carbonate platform ($A_{platform}$) in the GEOCLIM model [*Walker et al.*, 2002]. This surface is not corresponding to the shelf area that is never completely covered by carbonate platforms. Within the GEOCLIM model, we allow neritic carbonate to accumulate only on $A_{platform}$, while pelagic carbonate can accumulate on the total shelf area which is kept at a constant value. Indeed, *Walker et al.* [2002] suggest a maximum increase of the shelf surface by a factor of 2.2 during the Cenomanian, but this only affects the amount of pelagic carbonate being deposited on the shelf in GEOCLIM. This effect is negligible compared to the impact of the increase in $A_{platform}$ on the neritic flux. On the other hand, in the Ridgwell model, no difference is made between the surface available to neritic carbonate accumulation and the total shelf area.

[37] In order to test the impact of the fluctuating area available for carbonate platforms, i.e., $A_{platform}$, we performed sensitivity tests assuming holding $A_{platform}$ fixed at its present-day value (0.6×10^6 km^2). In this case, the calculated lysocline depth is always below its present-day level, which is an unrealistic result. Nevertheless, over-saturation of the seawater with respect to carbonate increases greatly, especially prior to Cretaceous times when it reaches an Ω_{ara} close to 9 (compared to 3 in the reference simulations) (Figure 9). However, the most striking difference is observed for the distribution of the carbonate deposition fluxes. Neritic accumulation remains identical between the sensitivity and reference runs up to the middle-late Triassic. Neritic accumulation then rapidly declines during the Early Jurassic and especially during the Cretaceous (Figure 7). This decline is directly linked to the expansion of calcareous nanoplankton that is not compensated for by high values of $A_{platform}$. However, this evolution is at odds with available data [*Wilkinson and Algeo*, 1989], that shows a rather constant continental carbonate accumulation throughout the Mesozoic (Figure 7c). The same discrepancy is observed for the deep-sea carbonate accumulation. The sensitivity tests show a rapid increase in this flux at the Jurassic-Cretaceous transition that is not observed in the data, while the reference run matches the data. We thus suggest that a large increase in $A_{platform}$ has occurred during the Mesozoic, since it explains the partition between neritic and deep sea carbonate deposition. It then seems to suggest that the supersaturation of the ocean relative to carbonate mineral was generally maintained at a low level (variable platform area scenario), with a lysocline depth relatively shallow. As mentioned above, the Mid-Cretaceous lysocline depth culminates at 400 m in the reference simulation. It is noteworthy that this lysocline depth falls to 5000 m if the area where carbonate platforms accumulate is maintained at its present-day value (Figure 9b). This illustrates the discrepancy existing between CCD depth reconstructions around 3500 m [*Tyrrell and Zeebe*, 2004; *Van Andel*, 1975], suggesting a large transfer of carbonate from the neritic environment to the deep sea during the Mid-Cretaceous, and carbonate accumulation fluxes on the seafloor which remain low until the end of the Cretaceous [*Wilkinson and Algeo*, 1989; *Wilkinson and Walker*, 1989]. This discrepancy might be at least partially solved by accounting for the existence of a transition zone between the lysocline and CCD whose thickness depends on the primary productivity in the photic zones among other parameters. For instance, the CCD depth in the Pacific Ocean is around 4200 m, while the Pacific lysocline is located at 1000 m. The difference between the CCD and the lysocline is much smaller for the Atlantic Ocean. Considering the extreme case, a lysocline at 400 m depth might correspond to a CCD depth of more than 3000 m, allowing accumulation of carbonate on the deep seafloor even with a shallow lysocline. Further-

more, GEOCLIM calculates a mean lysocline depth for the global mid- to low-latitude ocean, without accounting for possible fluctuations between oceanic basins.

5. Modeling Approaches: An Overview of the Limitations

[38] There are important limitations to this modeling exercise, the most critical of them being probably the assumption of a constant solid Earth degassing rate. As noted above, the long-term Earth degassing flux is a poorly known forcing; hence we have been led to a conservative approach. In addition, while spatial resolution of the weathering has been introduced, we chose to keep constant the fractions of silicate, basalt and carbonate outcrops for all time slices and for each grid element, these fractions being implicitly fitted through the adjustment of the calibration constants so that the control run reproduces the global measured alkalinity production through the weathering of these lithologies. Indeed, *Gibbs et al.* [1999] have demonstrated the weak influence of changes in lithology since 250 Ma on the calculation of the weathering fluxes. This result, although surprising, is mainly the consequence of the rather constant zonal relative abundance of each lithological type. Second, our aim was to introduce a minimum of uncertainties in our modeling exercise in order to firmly establish the impact of the paleogeographical setting during the Mesozoic. So far as different working assumptions and formulations can be used when trying to unravel the long-term carbon cycle, a good knowledge of the model structure is an important consideration. The traditional approach is to account for most of the processes included in the carbon cycle; however, in this case, empirical and less explicitly resolved formulations are often preferred to a more mechanistic approach. For example, in the Berner models [*Berner*, 1991, 1994; *Berner and Kothavala*, 2001], the organic carbon cycle in not explicitly resolved; rather it is forced by the reconstructed time evolution of the $\delta^{13}C$ as well as the impact of the continental drift, which is implicitly accounted for by adding multiplying factors in the weathering flux calculation (i.e., GEOG(t) and RUN). These choices keep the computational cost of the model moderate. A similar approach (similar in terms of inverse approach) is the one designed by *Rothman* [2002]. In this case, the strontium and carbon isotope signals are used for their shared dependence on the magmatic activity and weathering rates to deduce the fluctuations in atmospheric CO_2.

[39] The accuracy of such reasoning however requires that the signals used to reconstruct the variable of interest are well constrained in terms of spatial and temporal resolution. This might be a questionable approach for the carbon isotopic curve, since this signal is highly influenced by localized processes, such as high productivity in river deltas. As a result, the carbon isotopic data displays a large spread [*Veizer et al.*, 1999]. In addition, since the carbon isotopic data points are not equally distributed in time, it is difficult to mathematically define the validity of a running mean curve. For example, times of environmental crisis such as those of biologic extinctions are generally over sampled but they record events which pertain more to phenomena typical of the 100 kyr time-scale rather than the 10 Myr time-scale. However, the basis of any atmospheric CO_2 model is to compute a carbon cycle that is always close to or at (depending on the model type) steady state at a 10 Myr step (in order to prevent unrealistically large PCO_2 fluctuations).

[40] Furthermore, the widely used technique of inverse modeling to predict past atmospheric CO_2 (starting from data sets and use them as a forcing function of a numerical model of the carbon cycle) always comes up against the problem of determining the physical significance of the solutions found. Of course, solutions with negative or null partial pressure of CO_2, although they might be acceptable on a strict mathematical point of view, will be avoided. But what can be said about upper limits? Because only "light" physics is included into simple inverse model (mainly through parameterizations, for instance the link between continental air temperature and PCO_2), the physical significance of the solutions may be not guaranteed. This is why we think that a model as mechanistic as possible must be developed in order to constrain all the degrees of freedom of the carbon-climate system, even if all processes cannot be easily included at first and still require the use of non-mechanistic parametric laws (for weathering rates for instance).

[41] Here, we have chosen a fully explicit approach allowing simulation of the marine organic and inorganic cycle as well as the spatial distribution of silicate, basalt and carbonate weathering as a function of climate. This of course results in a less efficient model in terms of computational cost, but it has the main advantage of explicitly resolving

the equations for the marine subcycles of the inorganic and organic carbon, the oxygen and the phosphorus which are all tightly coupled to the atmospheric CO_2 content and to the weathering feedback. Our approach is in line with the one developed by *Bergman et al.* [2004], who emphasize the need for (1) including the coupling between the carbon, the oxygen and the sulphur cycle in order to build a consistent model of Earth system changes and (2) avoiding the use of $\delta^{13}C$ or other isotopic signal such as the $\delta^{34}S$ records as forcing functions. One of the future refinements of the GEOCLIM model will be to include the sulphur cycle. In its present form, only the coupling between the carbon, the phosphorus, the oxygen and the alkalinity cycles are included.

6. Conclusions

[42] In this study, we used the coupled climate-geochemical model GEOCLIM to investigate the role of the Pangea breakup on the Mesozoic climate evolution. The climate module of GEOCLIM is the FOAM GCM, while the global geochemical module is an improved version of the COMBINE model. The main conclusion is that the paleogeographical setting is a first order controlling factor of the geochemical carbon cycle and global climate, through its impact on continental runoff and on continental silicate weathering. From a global point of view, the climate is getting wetter and colder over the course of the Pangea breakup. Atmospheric CO_2 declines from 2420 ppmv in the early Permian down to 261 ppmv in the latest Cretaceous, with peak values reached during the early Triassic (3620 ppmv). Continental mean air temperature falls by about 9°C from 270 Ma to 65 Ma, while continental runoff increases by 20%. The first order driving force of this long term climatic evolution is the breakup of the Pangea supercontinent, which increases continental runoff above continents and CO_2 consumption through continental silicate weathering.

[43] However, this long term global cooling and CO_2 drawdown is not gentle, and is marked by a rapid cooling between the Middle-Late Triassic and the late Early Jurassic, mainly driven by a northward drift of Pangea (continental mean annual temperature falls by 5.4°C). This illustrates the nonlinear response of global climate to the paleogeographic evolution, showing that small paleogeographic changes may induce large climatic shift.

[44] Carbonate deposition appears to be strongly dependent on the paleogeographical configuration as well. In this study, because total CO_2 degassing is kept constant, only continental carbonate weathering controls the fluctuations calculated for the total carbonate burial flux. For instance, lowering of the carbonate weathering during the late Early Jurassic results in a minimum carbonate deposition for the last 270 million years. The causes of this minimum lie in the northward drift of Pangea, reducing strongly the alkalinity supply through continental carbonate dissolution from mid-southern latitudes. Correct modeling of past carbonate deposition thus requires a mechanistic modeling of the carbonate weathering rates.

[45] Further studies of the global biogeochemical cycles at the million year timescale should include the explicit calculation of the climate with a spatial resolution. We show here that the coupling between a geochemical model and a climate model is critical when attempting to estimate past PCO_2. We have found that, even with a constant CO_2 degassing rate, large fluctuations in the atmospheric PCO_2 are predicted, when paleogeographical forcing is explicitly taken into account. Integrated modeling should now include a history of the solid Earth degassing rate together with the paleogeographical forcing, once a consensus about this degassing history can be reached.

Acknowledgments

[46] This work was supported in part by the Climate Systems Center of the University of Chicago (US NSF grant ATM-0121028). Funding was also provided by the CNRS ECLIPSE program. We thank the Praksys team (http://www.praksys.org) for the maintenance of the cluster of PC of the LMTG, where geochemical coupled simulations were performed. We gratefully acknowledge use of "Jazz," a 350-node computing cluster operated by the Mathematics and Computer Science Division at Argonne National Laboratory as part of its Laboratory Computing Resource Center, where FOAM simulations were performed.

References

Bergman, N. M., T. M. Lenton, and A. J. Watson (2004), COPSE: A new model of biogeochemical cycling over Phanerozoic times, *Am. J. Sci.*, *304*, 397–437.

Berner, R. A. (1991), A model for atmospheric CO_2 over phanerozoic time, *Am. J. Sci.*, *291*, 339–376.

Berner, R. A. (1994), 3GEOCARB II: A revised model of atmosphere CO_2 over Phanerozoic time, *Am. J. Sci.*, *294*, 59–91.

Berner, R. A., and Z. Kothavala (2001), GEOCARB III: A revised model of atmospheric CO_2 over Phanerozoic time, *Am. J. Sci.*, *301*, 182–204.

Besse, J., and V. Courtillot (2002), Apparent and true polar wander and the geometry of the geomagnetic field over the last 200 Myr, *J. Geophys. Res.*, *107*(B11), 2300, doi:10.1029/2000JB000050.

Bown, P. R., M. K. E. Cooper, and A. R. Lord (1988), A calcareous nannofossil biozonation scheme for the Early to Mid Mesozoic, *Newsl. Stratigr.*, *20*(2), 91–114.

Brady, P. V. (1991), The effect of silicate weathering on global temperature and atmospheric CO_2, *J. Geophys. Res.*, *96*(B11), 18,101–18,106.

Brady, P. V., and S. A. Carroll (1994), Direct effects of CO_2 and temperature on silicate weathering: Possible implications for climate control, *Geochim. Cosmochim. Acta*, *58*(8), 1853–1856.

Catubig, N. R., D. E. Archer, R. Francois, P. deMenocal, W. Howard, and E. F. Yu (1998), Global deep-sea burial rate of calcium carbonate during the last glacial maximum, *Paleoceanography*, *13*, 298–310.

Cogné, J. P., and E. Humler (2004), Temporal variation of oceanic spreading and crustal production rates during the last 180 My, *Earth Planet. Sci. Lett.*, *227*, 427–439.

Crowley, T. J., and R. A. Berner (2001), Paleoclimate - CO_2 and climate change, *Science*, *292*, 870–872.

Dercourt, J., L. E. Ricou, and B. Vrielynck (1993), Atlas Tethys Paleoenvironmental Maps, explanatory notes, 307 pp., Gauthier-Villars, Paris.

Dessert, C., B. Dupré, L. M. François, J. Schott, J. Gaillardet, G. J. Chakrapani, and S. Bajpai (2001), Erosion of Deccan Traps determined by river geochemistry: Impact on the global climate and the $^{87}Sr/^{86}Sr$ ratio of seawater, *Earth Planet. Sci. Lett.*, *188*(3/4), 459–474.

Dessert, C., B. Dupré, J. Gaillardet, L. M. François, and C. J. Allègre (2003), Basalt weathering laws and the impact of basalt weathering on the global carbon cycle, *Chem. Geol.*, *202*, 257–273.

Donnadieu, Y., Y. Goddéris, G. Ramstein, A. Nédelec, and J. G. Meert (2004a), Snowball Earth triggered by continental break-up through changes in runoff, *Nature*, *428*, 303–306.

Donnadieu, Y., G. Ramstein, Y. Goddéris, and F. Fluteau (2004b), Global tectonic setting and climate of the Late Neoproterozoic: A climate-geochemical coupled study, in *The Extreme Proterozoic: Geology, Geochemistry, and Climate*, *Geophys. Monogr. Ser.*, vol. 146, edited by G. Jenkins et al., pp. 79–89, AGU, Washington, D. C.

Donnadieu, Y., R. T. Pierrehumbert, F. Fluteau, and R. Jacob (2006), Modelling the primary control of paleogeography on Cretaceous climate, *Earth Planet. Sci. Lett.*, *248*, 426–437.

Engebretson, D. C., K. P. Kelley, H. J. Cashman, and M. A. Richards (1992), 180 million years of subduction, *GSA Today*, *2*, 93–95.

François, L. M., and Y. Goddéris (1998), Isotopic constraints on the Cenozoic evolution of the carbon cycle, *Chem. Geol.*, *145*, 177–212.

François, L. M., and J. C. G. Walker (1992), Modelling the Phanerozoic carbon cycle and climate: Constraints from the $^{87}Sr/^{86}Sr$ isotopic ratio of seawater, *Am. J. Sci.*, *292*, 81–135.

François, L. M., J. C. G. Walker, and B. N. Opdyke (1993), The history of global weathering and the chemical evolution of the ocean-atmosphere system, in *Evolution of the Earth and Planets*, *Geophys. Monogr. Ser.*, vol. 74, edited by E. Takahashi, R. Jeanloz, and D. Dubie, pp. 143–159, AGU, Washington, D. C.

Gaffin, S. (1987), Ridge volume dependence on seafloor generation rate and inversion using long term sealevel change, *Am. J. Sci.*, *287*, 596–611.

Gaillardet, J., B. Dupré, P. Louvat, and C. J. Allègre (1999), Global silicate weathering and CO_2 consumption rates deduced from the chemistry of the large rivers, *Chem. Geol.*, *159*, 3–30.

Gibbs, M. T., G. J. S. Bluth, P. J. Fawcett, and L. R. Kump (1999), Global chemical erosion over the last 250 My: Variations due to changes in paleogeography, paleoclimate, and paleogeology, *Am. J. Sci.*, *299*, 611–651.

Goddéris, Y., and M. M. Joachimski (2004), Global change in the late Devonian: Modelling the Frasnian-Famennian short-term carbon isotope isotope excursions, *Palaeogeogr. Palaeoclimatol. Palaeoecol.*, *202*, 309–329.

Goddéris, Y., L. M. François, and J. Veizer (2001), The early Paleozoic carbon cycle, *Earth Planet. Sci. Lett.*, *190*, 181–196.

Goddéris, Y., Y. Donnadieu, C. Dessert, B. Dupré, F. Fluteau, L. M. François, A. Nédélec, and G. Ramstein (2005), Coupled modelling of global carbon cycle and climate in the Neoproterozoic: Links between Rodinia breakup and major glaciations, *C. R. Geosci.*, in press.

Gough, D. O. (1981), Solar interior structure and luminosity variations, *Sol. Phys.*, *74*, 21–34.

Guidry, M. W., and F. T. MacKenzie (2000), Apatite weathering and the Phanerozoic phosphorus cycle, *Geology*, *28*, 631–634.

Guidry, M. W., and F. T. Mackenzie (2003), Experimental study of igneous and sedimentary apatite dissolution: Control of pH, distance from equilibrium, and temperature on dissolution rates, *Geochim. Cosmochim. Acta*, *67*, 2949–2963.

Gwiazda, R. H., and W. S. Broecker (1994), The separate and combined effect of temperature, soil pCO_2, and organic acidity on silicate weathering in the soil environment: Formulation of a model and results, *Global Biogeochemical. Cycles*, *8*(2), 141–155.

Hardie, L. A. (1996), Secular variation in seawater chemistry: An explanation for the coupled secular variation in the mineralogy of marine limestones and potash evaporites over the past 600 my, *Geology*, *24*, 279–283.

Horita, J., H. Zimmermann, and H. D. Holland (2002), Chemical composition of seawater during the Phanerozoic: Implications from the record of marine evaporites, *Geochim. Cosmochim. Acta*, *66*(21), 3733–3756.

Jacob, R. (1997), Low frequency variability in a simulated atmosphere ocean system, Type thesis, Univ. of Wisconsin-Madison, Madison.

Kuznetsova, K. I. (2003), The first genera of planktonic foraminifers: Morphogenesis, development, and expansion in the Jurassic, *Paleontol. J.*, *37*(5), 472–485.

Labat, D., Y. Goddéris, J. L. Probst, and J. L. Guyot (2004), Evidence for global runoff increase related to climate warming, *Adv. Water Resour.*, *27*, 631–642.

Lemoine, M., et al. (1986), The continental margin of the Mesozoic Tethys in the Western Alps, *Mar. Pet. Geol.*, *3*, 179–199.

Lieth, H. (1984), Biomass pools and primary productivity of natural and managed ecosystem types in global perspective, in *Option Méditerranée 1984 Workshop*, pp. 7–14, Cent. Int. de Hautes Etud. Agron. Mediter., Paris.

Milliman, J. D. (1993), Production and accumulation of calcium carbonate in the ocean: Budget of a non steady-state, *Global Biogeochemical, Cycles*, *7*, 927–957.

Millot, R., J. Gaillardet, B. Dupré, and C. J. Allègre (2002), The global control of silicate weathering rates and the coupling with physical erosion: New insights from rivers of the Canadian Shield, *Earth Planet. Sci. Lett.*, *196*, 83–98.

Oliva, P., J. Viers, and B. Dupré (2003), Chemical weathering in granitic crystalline environments, *Chem. Geol.*, *202*, 225–256.

Opdyke, B. N., and B. H. Wilkinson (1993), Carbonate mineral saturation state and cratonic limestone accumulation, *Am. J. Sci.*, *293*, 217–234.

Petoukhov, V., A. Ganopolski, V. Brovkin, M. Claussen, A. Eliseev, C. Kubatzki, and S. Rahmstorf (2000), CLIMBER-2: A climate system model of intermediate complexity. Part I: Model description and performance for present climate, *Clim. Dyn.*, *16*, 1–17.

Petsch, S. T., and R. A. Berner (1998), Coupling the geochemical cycles of C, P, Fe, and S: The effect on atmospheric O_2 and the isotopic records of carbon and sulfur, *Am. J. Sci.*, *298*, 246–262.

Poulsen, C. J. (2003), Absence of a runaway ice-albedo feedback in the Neoproterozoic, *Geology*, *31*, 115–118.

Poulsen, C. J., E. J. Barron, C. C. Johnson, and P. J. Fawcett (1999), Links between the major climatic factors and regional oceanography in the mid-Cretaceous, in *Evolution of the Cretaceous Ocean-Climate System*, edited by E. Barrera and C. C. Johnson, *Spec. Pap. Geol. Soc. Am.*, *332*, 73–90.

Poulsen, C. J., R. T. Pierrehumbert, and R. L. Jacob (2001), Impact of ocean dynamics on the simulation of the Neoproterozoic "snowball Earth", *Geophys. Res. Lett.*, *28*, 1575–1578.

Poulsen, C. J., R. L. Jacob, R. T. Pierrehumbert, and T. T. Huynh (2002), Testing paleogeographic controls on a Neoproterozoic snowball Earth, *Geophys. Res. Lett.*, *29*(11), 1515, doi:10.1029/2001GL014352.

Ridgwell, A. J. (2005), A mid Mesozoic revolution in the regulation of ocean chemistry, *Mar. Geol.*, *217*, 339–357.

Ridgwell, A. J., M. J. Kennedy, and K. Caldeira (2003), Carbonate deposition, climate stability, and Neoproterozoic ice ages, *Science*, *302*, 859–862.

Ronov, A. B. (1982), The Earth's sedimentary shell (quantitative patterns of its structure, compositions, and evolution), *Int. Geol. Rev.*, *24*(11), 1313–1388.

Roth, P. H. (1986), Mesozoic paleoceanography of the North-Atlantic and the Tethys ocean, in *North Atlantic Paleoceanography*, edited by C. P. Summerhays and N. J. Shackleton, *Geol. Soc. Spec. Publ.*, *21*, 299–320.

Rothman, D. H. (2002), Atmospheric carbon dioxide levels for the last 500 million years, *Proc. Natl. Acad. Sci. U. S. A.*, *99*(7), 4167–4171.

Rowley, D. B. (2002), Rate of plate creation and destruction: 180 Ma to present, *Geol. Soc. Am. Bull.*, *114*(8), 927–933.

Royer, D. L. (2003), Estimating latest Cretaceous and Tertiary atmospheric CO_2 from stomatal indices, in *Causes and Consequences of Globally Warm Climates in the Early Paleogene*, edited by S. L. Wing et al., *Spec. Pap. Geol. Soc. Am.*, *369*, 23–33.

Royer, D. L. (2004), CO_2 as a primary driver of Phanerozoic climate, *GSA Today*, *14*, 4–10.

Royer, D. L., R. A. Berner, and D. J. Beerling (2001), Phanerozoic atmospheric CO_2 change: Evaluating geochemical and paleobiological approaches, *Earth Sci. Rev.*, *54*, 349–392.

Sandberg, P. A. (1983), An oscillating trend in Phanerozoic nonskeletal carbonate mineralogy, *Nature*, *305*, 19–22.

Stoll, H. M., and D. P. Schrag (2000), High-resolution stable isotope records from the Upper Cretaceous rocks of Italy and Spain: Glacial episodes in a greenhouse planet?, *Geol. Soc. Am. Bull.*, *112*(2), 308–319.

Tyrrell, T., and R. E. Zeebe (2004), History of carbonate ion concentration over the last 100 million years, *Geochim. Cosmochim. Acta*, *68*(17), 3521–3530.

Usdowski, E. (1980), Sur quelques aspects physico-chimiques de la formation des carbonates naturels, in *Géochimie des Interactions Entre les Eaux, les Minéraux et les Roches*, edited by Y. Tardy, pp. 49–99, SARL Elements, Tarbes, France.

Van Andel, T. H. (1975), Mesozoic/Cenozoic calcite compensation depth and the global distribution of calcareous sediments, *Earth Planet. Sci. Lett.*, *26*, 187–194.

Veizer, J., et al. (1999), $^{87}Sr/^{86}Sr$, $\delta^{13}C$ and $\delta^{18}O$ evolution of Phanerozoic seawater, *Chem. Geol.*, *161*, 59–88.

von Blanckenburg, F. (2005), The control mechanisms of erosion and weathering at basin scale from cosmogenic nuclides in river sediment, *Earth Planet. Sci. Lett.*, *237*, 462–479.

Walker, J. C. G., P. B. Hays, and J. F. Kasting (1981), A negative feedback mechanism for the long-term stabilization of Earth's surface temperature, *J. Geophys. Res.*, *86*, 9776–9782.

Walker, L. J., B. H. Wilkinson, and L. C. Ivany (2002), Continental drift and Phanerozoic carbonate accumulation in shallow-shelf and deep-marine settings, *J. Geol.*, *110*, 75–87.

Wallman, K. (2001), Controls on the Cretaceous and Cenozoic evolution of seawater composition, atmospheric CO_2 and climate, *Geochim. Cosmochim. Acta*, *65*(18), 3005–3025.

Wilkinson, B. H., and T. J. Algeo (1989), Sedimentary carbonate record of calcium-magnesium cycling, *Am. J. Sci.*, *289*, 1158–1194.

Wilkinson, B. H., and J. C. G. Walker (1989), Phanerozoic cycling of sedimentary carbonates, *Am. J. Sci.*, *289*, 525–548.